Remote Sensing of Environment 113 (2009) 1293–1303

Contents lists available at ScienceDirect

Remote Sensing of Environment

journal homepage: www.elsevier.com/locate/rse

Detection of Rossby waves in multi-parameters in multi-mission satellite observations and HYCOM simulations in the Indian Ocean

Bulusu Subrahmanyam [a,*], David M. Heffner [b], David Cromwell [c], Jay F. Shriver [d]

[a] Marine Science Program & Dept. of Geological Sciences, University of South Carolina, Columbia, SC 29205, USA
[b] Dept. of Geological Sciences, University of South Carolina, Columbia, SC 29205, USA
[c] Ocean Observing and Climate Research Group, National Oceanography Centre, Southampton, S014 3ZH, UK
[d] Naval Research Laboratory, Stennis Space Center, Mississippi, USA

ARTICLE INFO

Article history:
Received 30 September 2008
Received in revised form 6 February 2009
Accepted 14 February 2009

Keywords:
Rossby waves
Indian Ocean
HYCOM
Satellite observations
SSH
SST
Ocean color

ABSTRACT

Rossby waves are difficult to detect with *in situ* methods. However, as we show in this paper, they can be clearly identified in multi-parameters in multi-mission satellite observations of sea surface height (SSH), sea surface temperature (SST) and ocean color observations of chlorophyll-*a* (chl-*a*), as well as 1/12° global HYbrid Coordinate Ocean Model (HYCOM) simulations of SSH, SST and sea surface salinity (SSS) in the Indian Ocean. While the surface structure of Rossby waves can be elucidated from comparisons of the signal in different sea surface parameters, models are needed to gain direct information about how these waves affect the ocean at depth. The first three baroclinic modes of the Rossby waves are inferred from the Fast Fourier Transform (FFT), and two-dimensional Radon Transform (2D RT). At many latitudes the first and second baroclinic mode Rossby wave phase speeds from satellite observations and model parameters are identified. Wavelet transforms of these multi-parameters from satellite observations and model simulations help to discriminate between the annual and semi-annual signal of these Rossby waves. This comprehensive study reveals that the surface signature of Rossby waves in SSS anomalies is likely to be between 0.05 and 0.3 psu in the South Indian Ocean.

1. Introduction

Rossby waves, a class of low-frequency waves owing their existence to the variation of the Coriolis parameter with latitude, have been clearly seen in sea surface height (SSH) measurements from altimetry (e.g. Chelton & Schlax, 1996; Cipollini et al., 1997; Cipollini et al., 2000; Fu, 2004; Perigaud & Delecluse, 1992; Polito & Liu, 2003; Subrahmanyam et al., 2001; Tokmakian & Challenor, 1993). Chelton and Schlax (1996) showed that oceanic Rossby waves are present throughout the world's oceans using SSH observations from TOPEX/Poseidon (T/P) altimetry. They also demonstrated that the standard linear theory for Rossby wave propagation was lacking as it could not account for the observed phase speeds which were in general higher than predicted, by a factor greater than 2 in some parts of the ocean. Killworth et al. (1997) extended the theory to account for the mean background flow and Killworth and Blundell (2003a,b) (hereafter KB2003) further extended it to include the combined effect of mean flow and topographic slope. These extensions, especially the mean flow, resolve most of the discrepancy between theory and observation.

Recent studies have demonstrated that aside from SSH, Rossby waves can be detected in sea surface temperature (SST) data from infrared sensors (Cipollini et al., 1997; Hill et al., 2000) and ocean color data (chlorophyll-*a* concentrations) (e.g. Cipollini et al., 2001; Kawamiya & Oschlies, 2001; Machu et al., 1999). Cipollini et al. (1997) found evidence of mode 1 through mode 3 baroclinic Rossby waves, east of the Mid-Atlantic Ridge at 34°N, in the energy spectrum of SSH and SST data derived from satellites. They found that while the signal strength in SSH was strongest in the first (fastest) baroclinic mode, and progressively weaker in mode 2 and mode 3, the reverse was true with SST: the strongest mode was the slowest of the three (mode 3). However, in their analysis of global SST data using the Radon Transform to calculate propagation speeds, Hill et al. (2000) found clear evidence of first-mode baroclinic Rossby waves propagating in every ocean basin, with amplitudes between 0.1 and 1.5 K. They noted that it seems most likely that the SST signature is caused by the advection of a meridional temperature gradient because the clearest Rossby wave signals are found between 25°S and 40°S (where such gradients are largest). They also noted that mid-ocean ridges seem to have an impact on the phase of the waves. In some cases the waves are apparently delayed or dissipated altogether, and in other cases they seem to be generated at the ridges. They also noted that the wave characteristics in SST change with time. For example they show that in one case the phase speeds seem to change from year to year, and

* Corresponding author. Tel.: +1 803 777 2572; fax: +1 803 777 6610.
E-mail address: sbulusu@geol.sc.edu (B. Subrahmanyam).

0034-4257/$ – see front matter © 2009 Elsevier Inc. All rights reserved.
doi:10.1016/j.rse.2009.02.017

suggest that this might be explained by different modes being more apparent in different years as a result of the forcing. They also note several cases where seasonal changes seem to have an impact, with discontinuities existing in the wave patterns in autumn and winter; yet the phase structure is aligned across the discontinuity, suggesting that the wave has continued to propagate.

The appearance of Rossby waves in ocean color data may be due to several biophysical mechanisms (e.g. Charria et al., 2003, 2006; Cipollini et al., 2001; Killworth et al., 2004; Siegel, 2001; Uz et al., 2001). Cipollini et al. (2001) demonstrated that Rossby waves could be seen in the ocean color signal. Uz et al. (2001) correlated the ocean color signal with the SSH signal of Rossby waves, and concluded that the waves produced phytoplankton blooms through the upwelling of nutrient rich water, a process dubbed the *Rossby rototiller* by Siegel (2001). The basic idea behind the *Rossby rototiller* is that by altering the pycnocline, these waves also impact the nutricline, upwelling nutrient rich water into the photic zone. Unlike eddies, the Rossby waves do not transport water masses with them, so they should be able to lift nutrients closer to the surface as they propagate, "turning over" the water masses in their path (Siegel, 2001). However several other authors pointed out that there may be other processes at work, and that the ocean color signal of the Rossby waves might not be new production at all, but rather old phytoplankton made more visible by the waves, or even simply dissolved organic material that appears to be chlorophyll to satellites (Dandonneau et al., 2003; Killworth et al., 2004).

Dandonneau et al. (2003) proposed that the ocean color signal of Rossby waves could not possibly be from upwelling, since the positive ocean color anomalies corresponded to positive SSH anomalies, which would indicate downwelling. Instead, they suggested that the ocean color signal was not actually chlorophyll, but rather floating particulate organic material that simply appeared to be chlorophyll because of its absorption of blue light, and reflectance of green. In this case, the waves may be acting as a "hay rake" in that they gather the floating organic material into rows at the surface. Killworth et al. (2004) rebutted the "hay rake" hypothesis, stating that planetary waves do not cause particles to converge in a plane. They proposed that the cause of the signal was physical processes, either through horizontal or vertical advection of the phytoplankton, and not caused by new growth at all. In the case of vertical advection, the waves would simply act to bring phytoplankton at depth closer to the surface where they would be more visible to a satellite. The horizontal advection hypothesis is that the signal is merely a perturbation in an ocean color gradient along the sea surface.

Killworth et al. (2004) concluded that nutrient pumping could not account for the phase lag of the ocean color signal with respect to the sea surface height signal. Since the two signals were basically coincident, it would require that the phytoplankton assimilated the nutrients almost instantaneously. They therefore proposed that the horizontal advection of phytoplankton is the dominant cause of the signal, but that vertical advection may account for some of the effects. In a later study Charria et al. (2006) used wavelet analysis and determined that new production could account for 50% of the signal, with the rest being explained by horizontal advection.

Quartly et al. (2003) compared SSH, SST, and ocean color Rossby wave signals in the Indian Ocean. They reported an amplitude in the SST signal at 34°S of about 0.5 K, and an SSH amplitude of about 5 cm. They note that the parameters at this latitude are all out of phase, with the Rossby wave signal in SST leading SSH which in turn leads the ocean color. They also noted that most of the faster moving features in SST and ocean color (presumably lower-mode baroclinic Rossby waves) have corresponding signals in SSH. But while there are slower moving signals (higher mode Rossby waves) in SST and ocean color, there does not appear to be an analogous slow moving signal in SSH. However they did observe that in the band between 15°S and 29°S the SST and ocean color signals were in phase. They reported that the ocean color signal was strongest in regions with a strong meridional gradient. However they observed that horizontal advection alone could not explain why the ocean color and SST signals were in phase north of 29°S. Interestingly, they also noted that the strongest Rossby wave signals in SSH and ocean color corresponded with each other south of 20°S but that the north of this latitude the dominant signal in ocean color favored higher-order mode Rossby waves, while the signal in SSH did not.

More recently, Heffner et al. (2008) used HYbrid Coordinate Ocean Model (HYCOM) simulations of sea surface salinity (SSS) to demonstrate that Rossby waves can be seen as a signal in salinity as well. We anticipate the high-density satellite measurements of salinity from space through future satellite missions Soil Moisture and Ocean Salinity (SMOS) and Aquarius missions will improve our knowledge of Rossby waves. The SMOS mission has been designed to observe soil moisture over the Earth's landmasses and salinity over the oceans. SMOS is planned for launch in April, 2009. It will yield global coverage every 3 days (Kerr et al., 2000). The Aquarius/SAC-D is a space mission developed by NASA and the Space Agency of Argentina (Comisión Nacional de Actividades Espaciales, CONAE), which is planned for launch in May, 2010. It will produce global salinity maps with 0.2 psu accuracy on a monthly basis (Lagerloef, 2001).

In this paper, we demonstrate that Rossby waves can be identified clearly in multi-parameter multi-satellite missions and we show comparisons with HYbrid Coordinate Ocean Model (HYCOM) derived parameters. Previous studies show that at 34°N the surface signature of the amplitude of Rossby waves in SSH is about 5 cm and about 0.5 K in the SST signal (Quartly et al., 2003). In global SST data, first-mode baroclinic mode Rossby wave surface amplitudes are roughly between 0.1 and 1.5 K (Hill et al., 2000). In this study we go further by investigating the amplitude of the surface signature of Rossby waves in chlorophyll concentration (chl-*a*) and sea surface salinity (SSS). We hope this study will provide a better understanding of the baroclinic structure of Rossby waves, through analysis of the comprehensive information of their impact on multiple parameters based on HYCOM model simulations and satellite data obtained for the period of 2003–2006. In Section 2, we discuss the multi-mission satellite data and HYCOM simulations. Section 3 presents the techniques we used in this study, namely the Fast Fourier Transform (FFT), Radon Transform (RT) and wavelet analysis; and Section 4 presents our results. Finally, in Section 5, we provide a summary and draw conclusions.

2. Satellite data and model simulations

2.1. Multi-mission satellite data

Sea surface height (SSH) data from Jason-1 altimetry, which encompasses January 2003 to December 2006, were obtained from the NASA-JPL Physical Oceanography Distributed Active Archive Center (PODAAC). In this study we use 1/2° gridded SSH anomaly data. Merged Ocean Color–Level 3 chlorophyll-*a* (chl-*a*) data with a weekly temporal resolution, and a 9 km spatial resolution, were obtained from ICESS at the University of California at Santa Barbara (Maritorena et al., submitted for publication). Sea surface temperature (SST) data from the GODAE High Resolution Sea Surface Temperature Pilot Project (GHRSST-PP) product of Operational SST and sea Ice Analysis (OSTIA) Level-4 data with a spatial resolution of 1/4° and daily temporal resolution were obtained from the National Centre for Ocean Forecasting.

2.2. HYCOM simulations

In this study we use global HYbrid Coordinate Ocean Model (HYCOM) simulations from 1/12° horizontal resolution (~7 km at mid-latitudes) and 32 hybrid layers in the vertical. The model is configured on a Mercator grid from 78°S to 47°N, with a bipolar grid

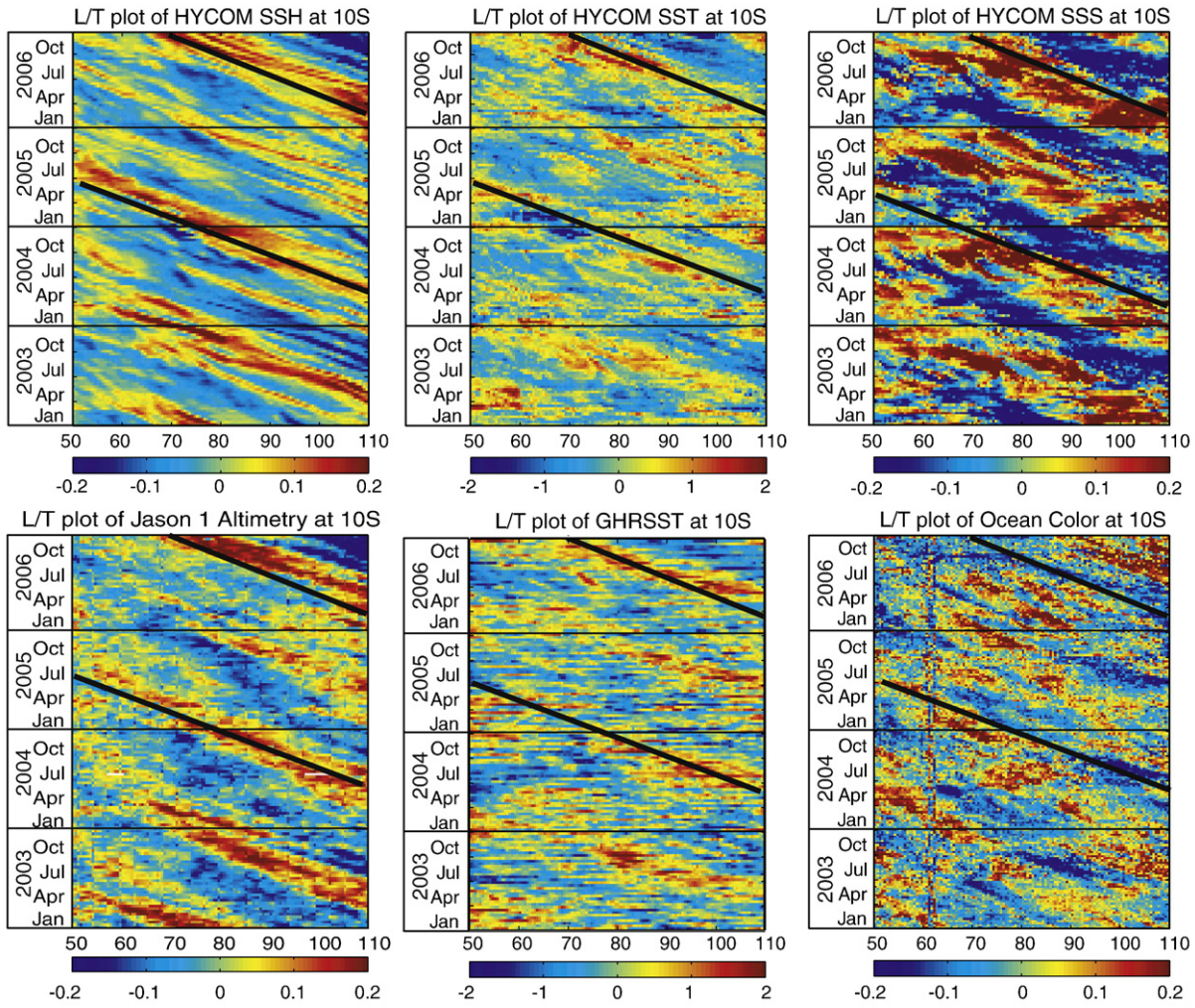

Fig. 1. Longitude–time plots at 10°S of parameter anomalies. (Top panel) HYCOM simulations of SSH, SST, SSS, and (bottom panel) satellite-derived parameters of Jason-1 altimetry, GHRSST, and Log of chl-*a* concentration. The solid lines represent Rossby waves' propagation.

used north of 47°N. Monthly mean temperature and salinity from the Generalized Digital Environmental Model (GDEM) climatology in August were used to initialize the model. This model was forced by 3 hourly Navy Operational Global Atmospheric Prediction System (NOGAPS) winds, heat fluxes and precipitation fields. This version of the model uses the NASA Goddard Institute for Space Studies level 2 (GISS) mixed layer scheme and includes monthly river runoff from 986 global rivers. There is a weak relaxation to monthly mean SSS from the Polar science center Hydrographic Climatology (PHC). There is no assimilation of any ocean data, including SST, and no relaxation to any other data except sea surface salinity (SSS) to keep the evaporation minus precipitation balance from deviating far from reality. The actual SSS relaxation e-folding time depends on the mixed layer depth (MLD) and is (30 days × MLD m/30 m) days, i.e. it is more rapid when the mixed layer is shallow and less so when it is deep. Heffner et al. (2008) used this version of the model, and from the simulations of salinity they showed detection of Rossby waves in salinity in the Indian Ocean. In this study we use the same version of the model, but include SSH and SST in addition to SSS.

3. Methodology

Jason-1 altimetry SSH anomalies, GHRSST, and the HYCOM simulations (SST, SSS, and SSH) were plotted on the same temporal (10-day) spacing, whereas chlorophyll-*a* data were plotted on an 8-day temporal resolution. All of the parameters were plotted at the same spatial (0.5° × 0.5°) resolution. All of these parameters were detrended in time and space by subtracting the 4-year mean for each point, and then subtracting the longitudinal mean (at a given time) for each point in order to remove seasonal and spatial trends. The zonal gradients of the detrended (anomaly) data were taken by subtracting the value at each point from the point on the left (west) and dividing by the spatial resolution in kilometers (to get a gradient in kilometers). These longitude/time gradient grids were then used in the Radon Transform (RT) and Fast Fourier Transform (FFT) techniques as outlined below.

The Radon Transform (RT) is a technique that projects the longitude–time (L/T) plot (or Hovmöller diagram) onto a line at angle theta to the x-axis. The sum of the squares of the values on the projected line will be greatest when the line is perpendicular to the direction of Rossby wave propagation (Challenor et al., 2001; Deans, 1983), and the speed can be calculated simply by taking the tangent of theta. For this study, a 2-D RT was applied to the gradients of the parameter anomalies, and the speed calculated for the most energetic feature at each latitude. Additionally, a RT was used in conjunction with a sliding window to analyze how the speed of Rossby waves changes in each parameter as the waves propagate across a band of longitude. A 2D RT was again used with a sliding window of 10° longitude centered on the point of interest.

The Fast Fourier Transform (FFT) is a technique in which the L/T plot is transformed onto a wave number and frequency space, which highlights the different spectral components. The FFT has the advantage

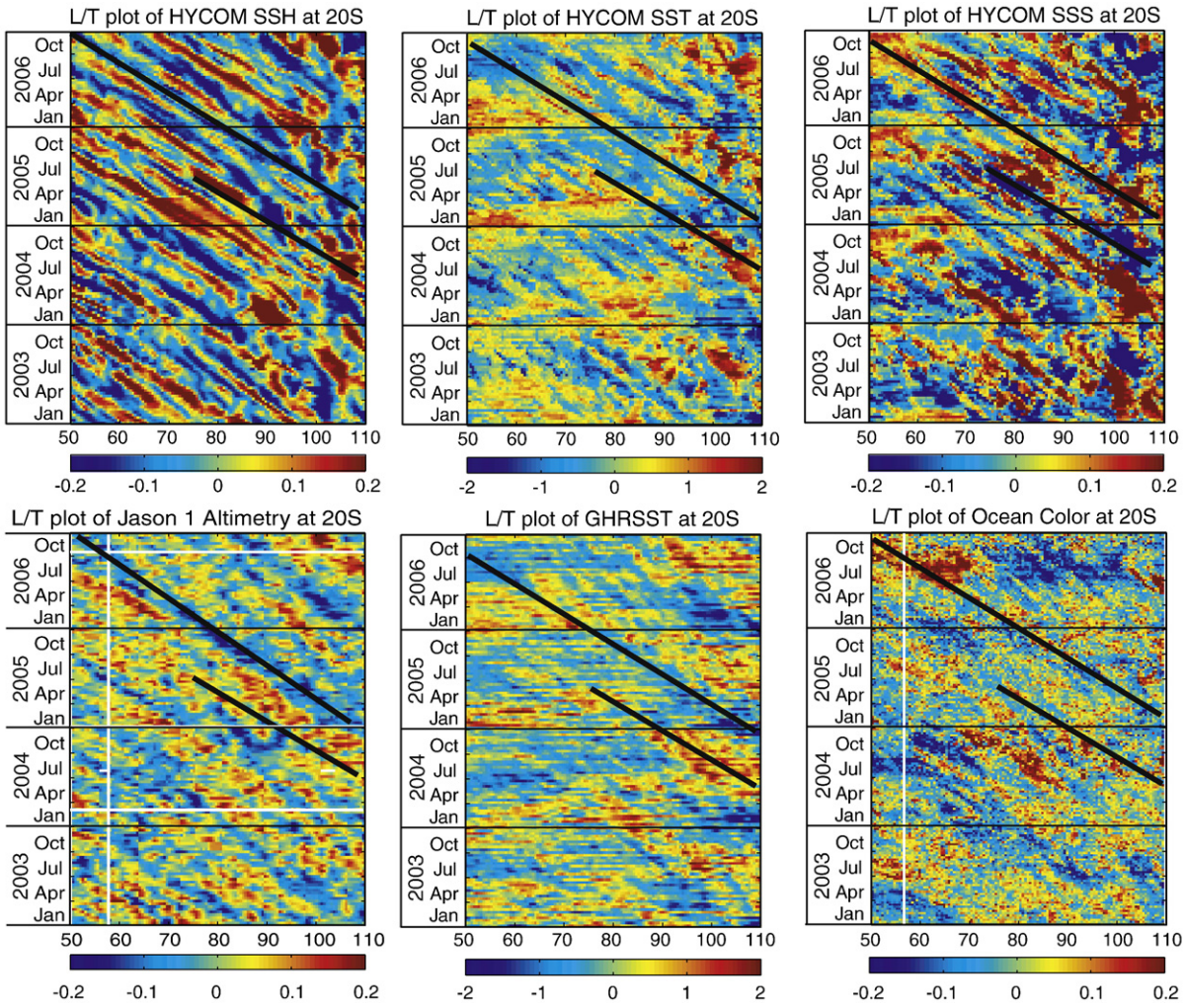

Fig. 2. Longitude–time plots at 20°S of parameter anomalies. (Top panel) HYCOM simulations of SSH, SST, SSS, and (bottom panel) satellite-derived parameters of Jason-1 altimetry, GHRSST, and Log of chl-*a* concentration. The solid lines represent Rossby waves' propagation.

of showing single components of a wave, which may translate to different baroclinic modes (Cipollini et al., 1997; Subrahmanyam et al., 2001). But because it maps a single wave frequency to each component, it requires that the propagation characteristics of the wave remain constant for the area and time being studied (Cipollini et al., 2000; Hill et al., 2000). The FFT is used to determine the wavelength, period, and amplitude of the first-mode baroclinic Rossby waves in the zonal gradient of each parameter. The wavelength and period are calculated by taking the inverse of the frequency components of the peak corresponding to the first-mode Rossby wave, then converted to kilometers and days respectively. The amplitude is calculated by dividing the absolute value of the Fourier Transform by one half of the product of the length of the x and y dimensions. The wavelength and period of the waves in the gradient are the same as in the parameter anomalies; however, the amplitude is not, and needs to be converted as outlined below:

$$h = A \cdot \cos(kx - \omega t) \tag{1}$$

$$k = \frac{2\pi}{L}. \tag{2}$$

Eq. (1) is the basic wave equation, where h is the value of the parameter as a function of space (x) and time (t). A is the amplitude of the wave, ω is the angular frequency, and k is the wave number which relates to the wavelength as shown in Eq. (2). Taking the zonal gradient of the parameter h, we have:

$$\frac{\partial h}{\partial x} = -A' \cdot \sin(kx - \omega t) \tag{3}$$

$$A' = Ak \tag{4}$$

$$A = A' \frac{L}{2\pi} \tag{5}$$

where A' is the amplitude of the gradient. Eq. (5) can be used to convert the gradient's amplitude into the parameter's amplitude.

Finally, we use wavelet analysis which is another technique similar to the FFT, in which a one dimensional time series is decomposed into its frequency components, based on the convolution of the original time series with a set of wavelet functions (Graps, 1995; Meyers et al., 1993; Torrence & Compo, 1998). The wavelet method allows one to analyze localized power variations within a discrete time series at a range of scales (Foufoula-Georgiou & Kumar, 1994). The local wavelet power spectrum is the square of the wavelet coefficients (Torrence & Compo, 1998). The global wavelet spectrum is the average spectrum over the complete time series, equivalent to the Fourier spectrum. This technique allow us to separate out the annual and semi-annual Rossby wave signals and help locate how the various period components might be changing in time and space (by performing wavelet analysis

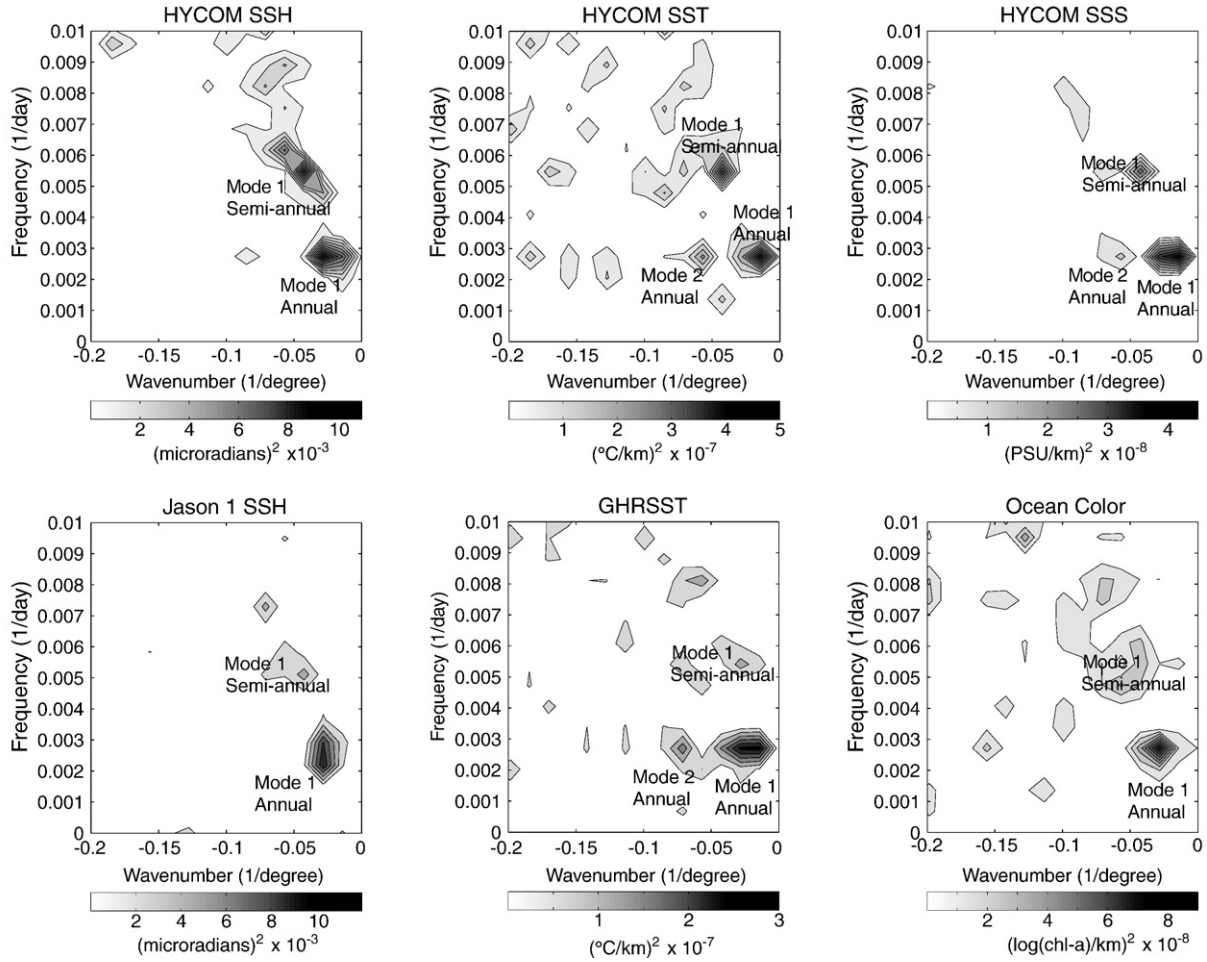

Fig. 3. Fast Fourier Transform (FFT) of (top panel) HYCOM simulations, and (bottom panel) satellite-derived parameter gradients from longitude/time plots at 10°S.

over, e.g., a range of longitudes for a fixed time and latitude). This type of analysis was used by Cromwell (2001) to study the effects of the mid-Atlantic ridge on baroclinic Rossby waves.

For the present study, a temporal wavelet analysis is carried out by applying the wavelet analysis to a time series of data anomalies extracted at 10°S for longitudes 60°E (western southern Indian Ocean) and 90°E (eastern southern Indian Ocean) at a temporal resolution of 10 days for each parameter except ocean color which has an 8-day resolution. The 95% significant curves are based on white noise. Additionally, wavelet analysis is used to investigate the effects of the 90 East ridge both on period and wavelength of the Rossby waves. For the temporal analysis, three latitudes were analyzed (10°S, 15°S, and 20°S) and for each latitude, five time series were used for each parameter (every 2° from 84°E–94°E). The spatial analysis was performed at a latitude of 20°S for each parameter at four different times (January 2004 and 2005, and June 2004 and 2005). The longitude series for the analysis had a resolution of 0.5° for each parameter.

Table 1
Signal properties of the Rossby wave baroclinic modes from HYCOM simulations and satellite observations calculated from a Fast Fourier Transforms (FFT) of the parameter gradients at 10°S.

Parameter	Mode	L (km)	T (days)	c (km/day)
HYCOM				
SSH	Mode 1	5470	370	14.8
	Mode 2	2430	192	12.6
SST	Mode 1	8400	370	22.7
	Mode 2	2730	182	15
	Mode 3	1820	370	4.9
SSS	Mode 1	8400	370	22.7
	Mode 2	2730	182	15
	Mode 3	1820	370	4.9
Satellite				
Jason-1 SSH	Mode 1	5470	360	15.3
	Mode 2	2430	200	12.2
GHRSST	Mode 1	7300	360	20.4
	Mode 2	3130	190	16.6
	Mode 3	1560	360	4.4
Ocean Color	Mode 1	5470	360	15.3

Table 2
First-mode baroclinic Rossby wave characteristics in different parameters derived from satellite observations and HYCOM simulations.

Parameter	10° S				10°S–30°S
	Amplitude of gradient	Wavelength (L) (km)	Period (T) (days)	Surface amplitude	Surface amplitude range
HYCOM SSS	0.0002199	5500	365	0.19 psu	0.03–0.30 psu
HYCOM SSH	0.0105	4000	365	6.68 cm	3.23–6.68 cm
HYCOM SST	0.000709	5500	365	0.62 °C	0.33–0.62 °C
Jason-1 SSH	0.01097	4000	415	6.98 cm	2.98–6.98 cm
GHRSST	0.00057	5500	365	0.50 °C	0.45–0.57 °C
Chlorophyll-*a*	0.000301	4000	365	1.21 mg/m^3	1.06–1.21 mg/m^3

These results are calculated from the Fast Fourier Transforms (FFT) at 10°S and between 10°S and 30°S.

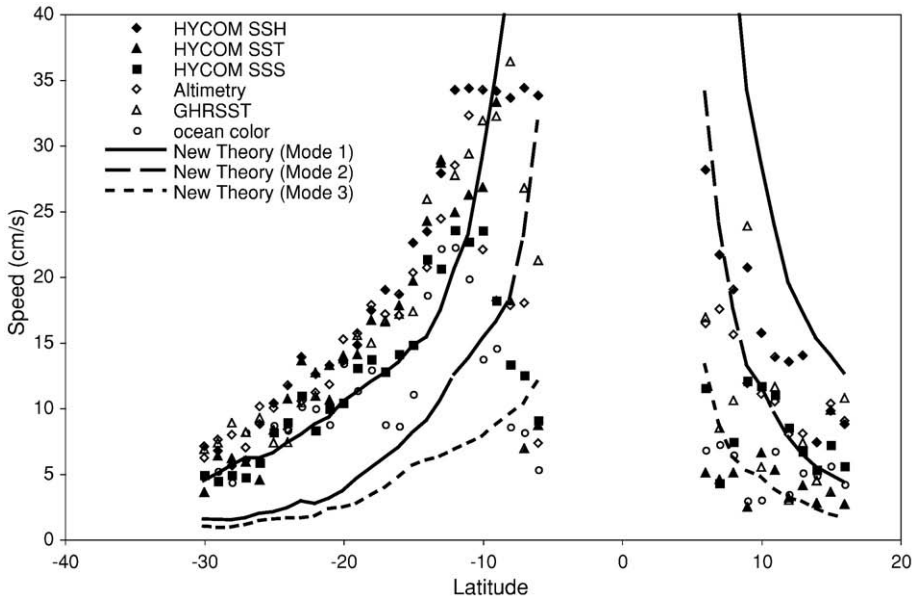

Fig. 4. Rossby wave speeds for each parameter calculated by a 2D Radon Transform (2D RT) at each degree of latitude from 30°S to 16°N (calculated from longitude/time plots of parameter gradients). The dark lines are the theoretical Rossby wave phase speeds calculated by Killworth and Blundell (2003a,b) (solid — mode 1; long dashed — mode 2; short dashed — mode 3).

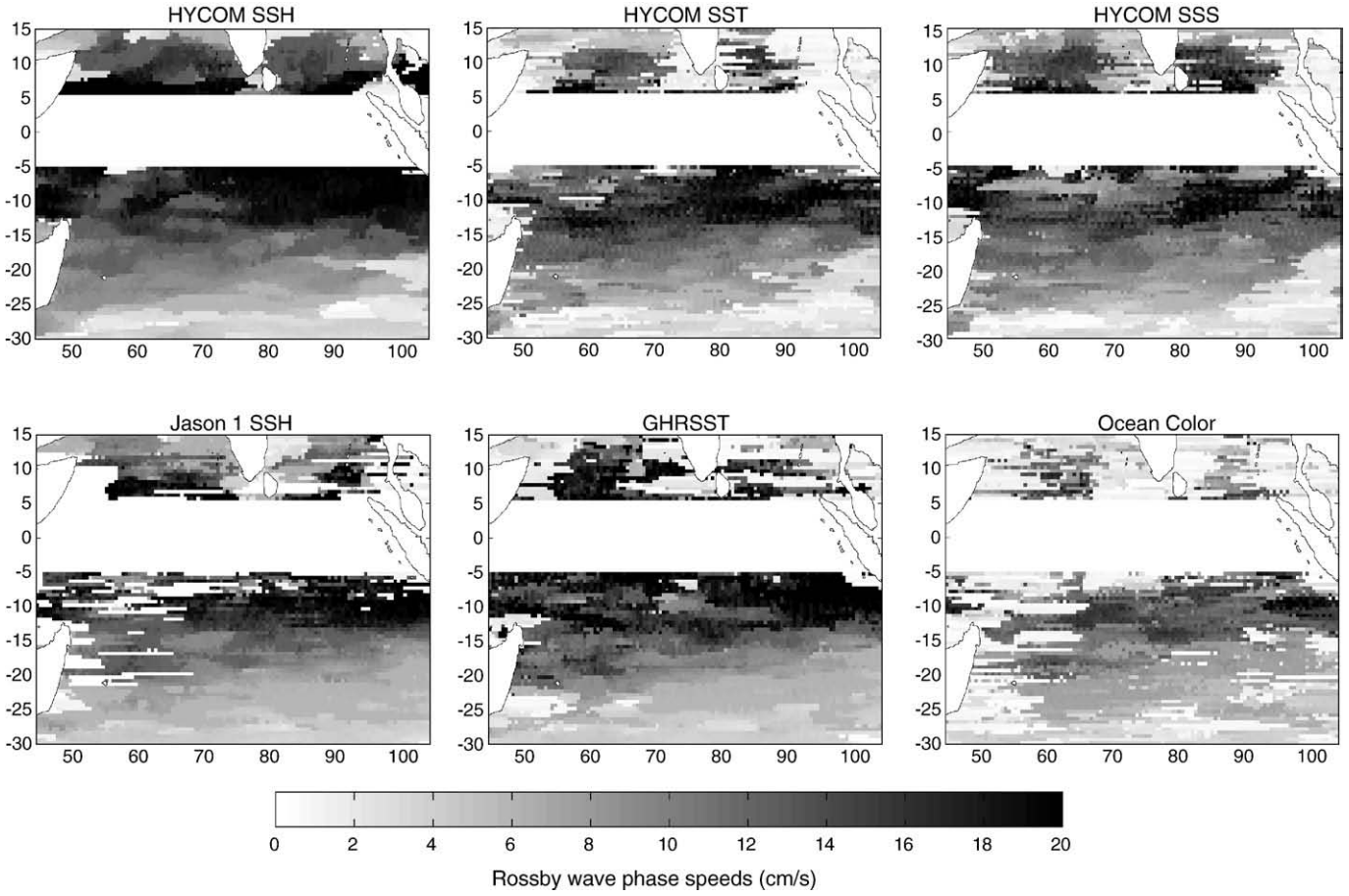

Fig. 5. Rossby wave phase speeds for (top panel) HYCOM simulations and (bottom panel) satellite-derived parameters calculated from a 2D Radon Transform (2D RT) on a sliding window.

4. Results and discussion

L/*T* plots along 10°S and 20°S of HYCOM simulations of SSH, SST and SSS (Figs. 1 and 2 top panel) and satellite observations of Jason-1 altimetry SSH, GHRSST and chl-*a* (Figs. 1 and 2 bottom panel) show clear propagation of Rossby waves from 2003–2006. In Fig. 1, the annual Rossby wave signal at 10°S can be clearly seen in HYCOM SSH and SSS, and Jason-1 altimetry. This signal is not as strong, but is still visible, in HYCOM SST, GHRSST, and ocean color chl-*a*. Also, with the exception of ocean color chl-*a*, all of the parameters appear to be in phase, where a propagating anomalous high in SSH, corresponds with a high in SST and SSS (this is true for both HYCOM and satellite-derived parameters). Ocean color chl-*a* however appears to be exactly 180° out of phase, where a propagating high anomaly corresponds with a propagating anomalously low chl-*a* concentration.

In Fig. 2, a very strong Rossby wave-like signal at 20°S is present in HYCOM SSH and SSS, and a weaker signal is present in all the other parameters. However, it is not clear from these diagrams whether it is an annual or semi-annual signal. The propagating SSH and SST anomalies appear to be in phase at this latitude, however HYCOM SSS and satellite-derived ocean color chl-*a* exhibit the opposite phase.

The power spectrum from the Fourier transform of each parameter at 10°S shows a strong peak with a period of about 1 year, and a wavelength in the 5500–8400 km range (Fig. 3 and Table 1). All of the parameters with the exception of ocean color also show a peak with a period of about half a year and a wavelength around 2500 km. We believe that these correspond to the first and second-mode baroclinic Rossby waves coinciding with the theoretical values of Killworth and Blundell (2003a, b). There does appear to be some overlap in the speeds as shown in Table 1: 14.8–22.7 km/d for mode 1; and 12.2–15 km/d for mode 2. The theoretical speeds in this basin at 10°S are 25 km/d for mode 1 and 13 km/d for mode 2. This discrepancy is possibly due to one or both of the following causes: 1) the true wavelength and periods of the features may fall in-between two of the Fourier Transform bins, thus giving a much larger range to the wavelengths and periods of the waves; 2) the surface expression of the waves in ocean color chl-*a* and sea surface height may be stronger in locations where the first-mode waves indeed have a shorter wavelength.

Table 2 presents the amplitude of the surface expression of the first-mode baroclinic waves in each parameter as calculated from the Fourier transform. The amplitudes in SSH and SST are comparable to the results reported by Quartly et al. (2003). Our calculated amplitude in HYCOM SSS of 0.03–0.3 psu suggests that the SMOS and Aquarius missions should be able to resolve Rossby waves in SSS at some latitudes.

The results of the Radon Transform (Fig. 4) for southern latitudes compare quite well with the new theoretical speed for Rossby waves

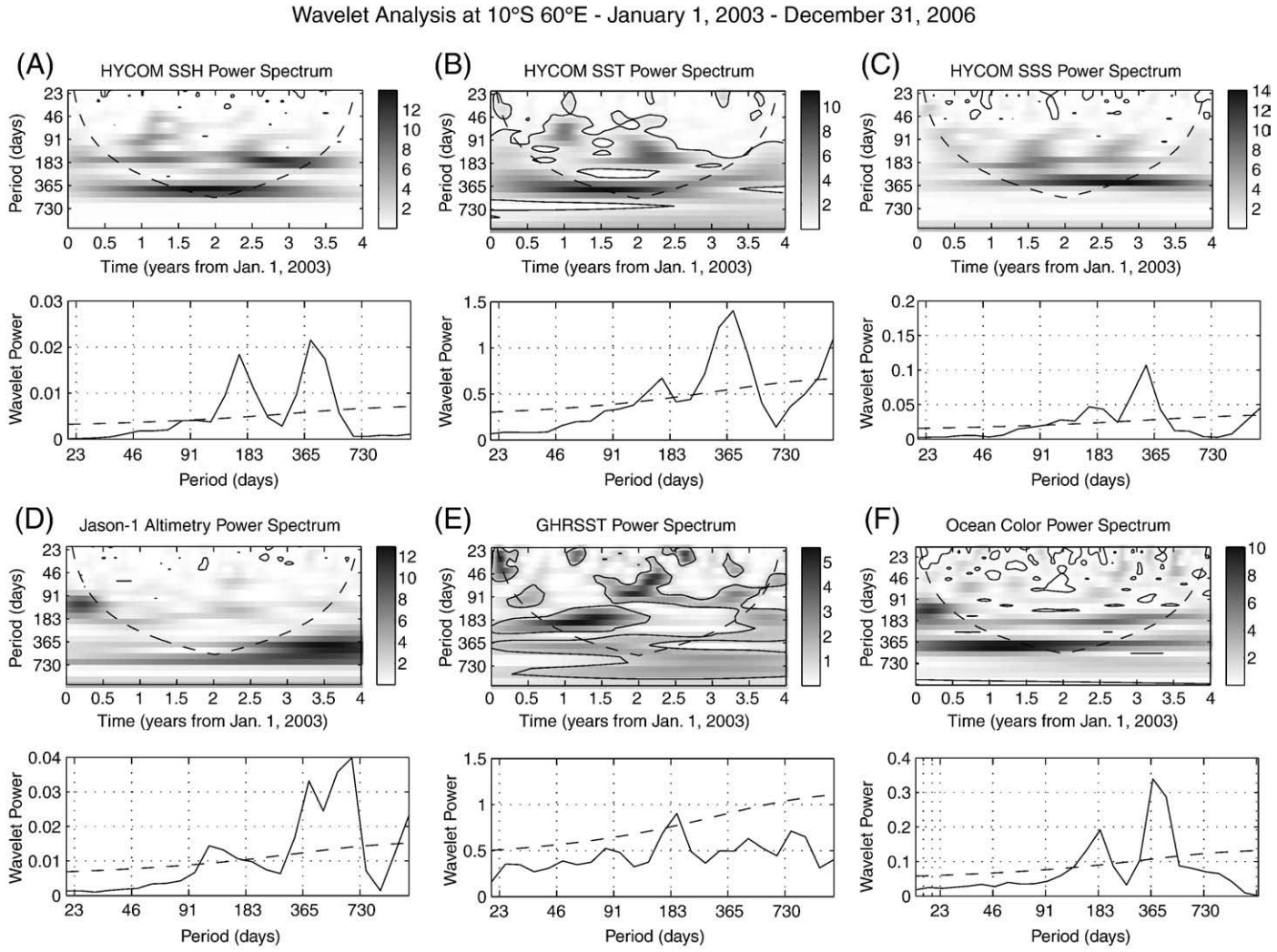

Fig. 6. Wavelet analysis of time series extracted from longitude/time plots of parameter anomalies at 10°S 60°E. The top diagram of each subplot is the wavelet power spectrum (how important a certain wave period is at a given time). The bottom diagram is of the global wavelet power (how important a particular period is relative to the whole time series). The dashed curve in the power spectrum figures is the cone of influence, below which edge effects become important and results have to be treated with caution. The dashed line in the global power diagrams is the 95% significance level (anything above is considered significant). A) HYCOM SSH, B) HYCOM SST, C) HYCOM SSS, D) Jason-1 altimetry, E) GHRSST, and F) ocean color (log of chl-*a* concentration).

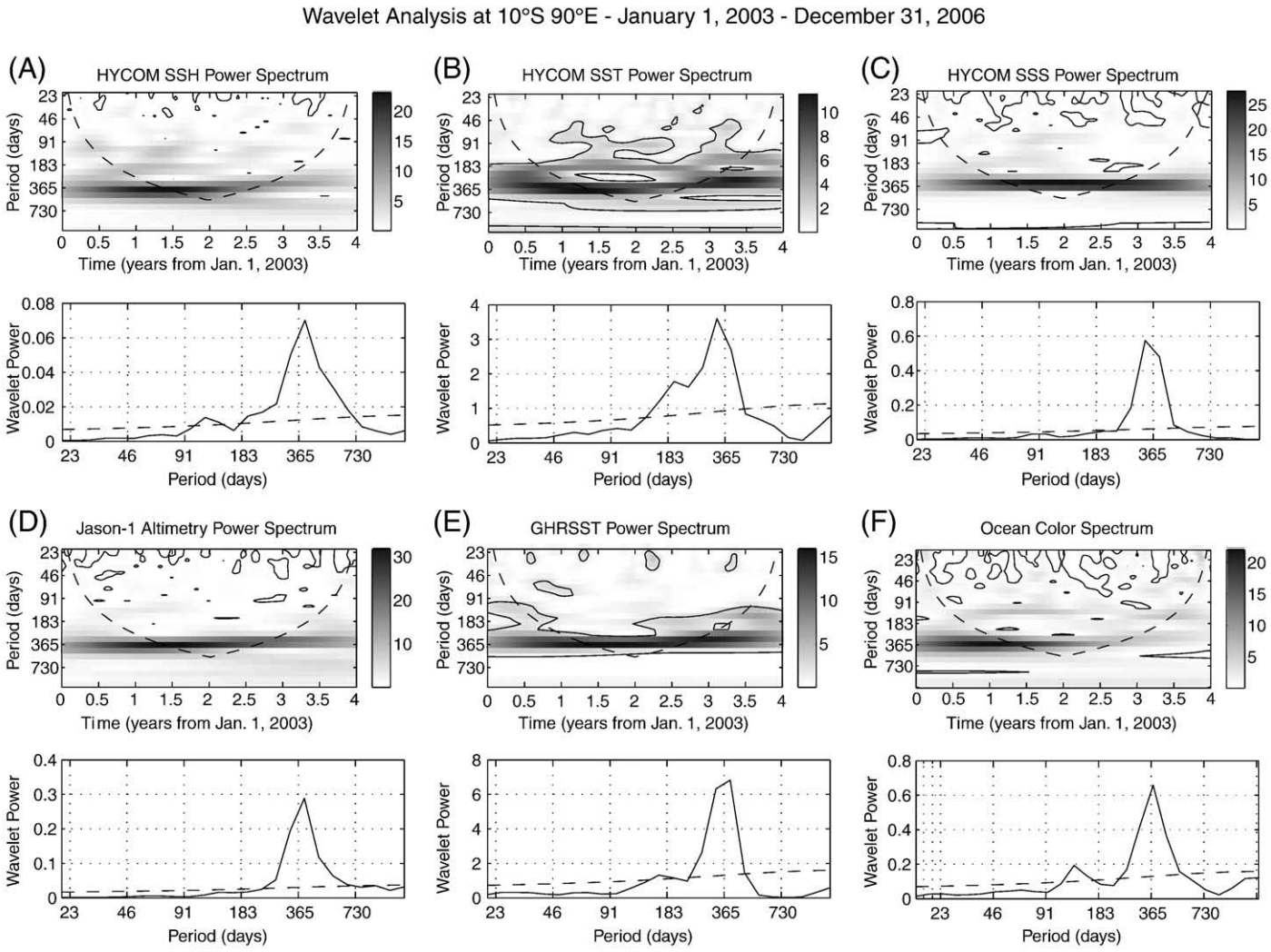

Fig. 7. Wavelet analysis of time series extracted from longitude/time plots of parameter anomalies at 10°S 90°E. The top diagram of each subplot is the wavelet power spectrum (how important a certain wave period is at a given time). The bottom diagram is of the global wavelet power (how important a particular period is relative to the whole time series). The dashed curve in the power spectrum figures is the cone of influence below which edge effects become important and results have to be treated with caution. The dashed line in the global power diagrams is the 95% significance level (anything above is considered significant). A) HYCOM SSH, B) HYCOM SST, C) HYCOM SSS, D) Jason-1 altimetry, E) GHRSST, and F) ocean color (log of chl-*a* concentration).

given by Killworth and Blundell (2003a,b). Yet interestingly none of the parameters in the northern latitudes match the predicted first-mode baroclinic Rossby wave speeds. Heffner et al. (2008) proposed that the reason Radon Transform showed that the phase speed of the Northern Hemisphere Rossby waves did not match the predicted first-mode Baroclinic speeds was that we had treated the two basins as one ocean, instead of separating them. However, during the Radon Transform exercise for this study, we did indeed separate the two basins (figure not shown), and found that while HYCOM SSS at 10°N–18°N in the Arabian Sea did track closer to first mode, this was not true for other parameters. Additionally, none of the parameters in the Bay of Bengal tracked along the baroclinic first-mode speeds.

In Fig. 5 it can be seen that the 2D RT on a sliding window was unable to resolve large portions of the Northern Hemisphere Rossby waves in satellite-derived parameters. HYCOM SST and SSS also appear quite noisy, but all subplots seem to show a general trend that matches the HYCOM SSH speed map. From the cleaner HYCOM SSH map, we can see that Rossby waves in the Northern Hemisphere indeed do appear to traverse more slowly than those features at comparable latitudes in the Southern Hemisphere. And even more interesting is that in Fig. 4, if the Northern HYCOM SSH phase speeds are shifted 5° to the North, they match the predicted Mode 1 phase speeds.

The Rossby wave speed map (Fig. 5) shows a general pattern of faster phase speeds toward the equator, gradating to much slower speeds in the mid-latitudes (a 10° band centered around the equator has been blocked out). Interestingly there seems to be a sharper zonal gradient of the speeds in the eastern part of the basin compared to the west. This change shows up clearest in the HYCOM (upper part of Fig. 5) parameters where the band of speeds from 5–12 cm/s occupies a range from about 18°S–15°S at 100°E, but this same band extends from 25°S–12°S by 50°E. The same trend can be seen in the satellite-derived parameters (lower part of Fig. 5), however there is somewhat more noise.

The results of the temporal wavelet transform (Figs. 6 and 7) clearly show a semi-annual and annual signal. These seem to correspond with the first and second baroclinic modes respectively, as pointed out in Fig. 3 and Table 1. It is interesting to note that the semi-annual signal is rather strong in the western part of the basin, especially in HYCOM SSH and satellite-derived ocean color, where its peak in the wavelet spectrum is comparable to the annual signal (Fig. 6). In the eastern part of the basin, the semi-annual signal is rather weak with a small peak compared to the strong annual signal (Fig. 7). Also, interestingly with the exception of Jason-1 altimetry in the west, all other parameters in both parts of the ocean have their strongest signals in July 2004 (~1.5 years).

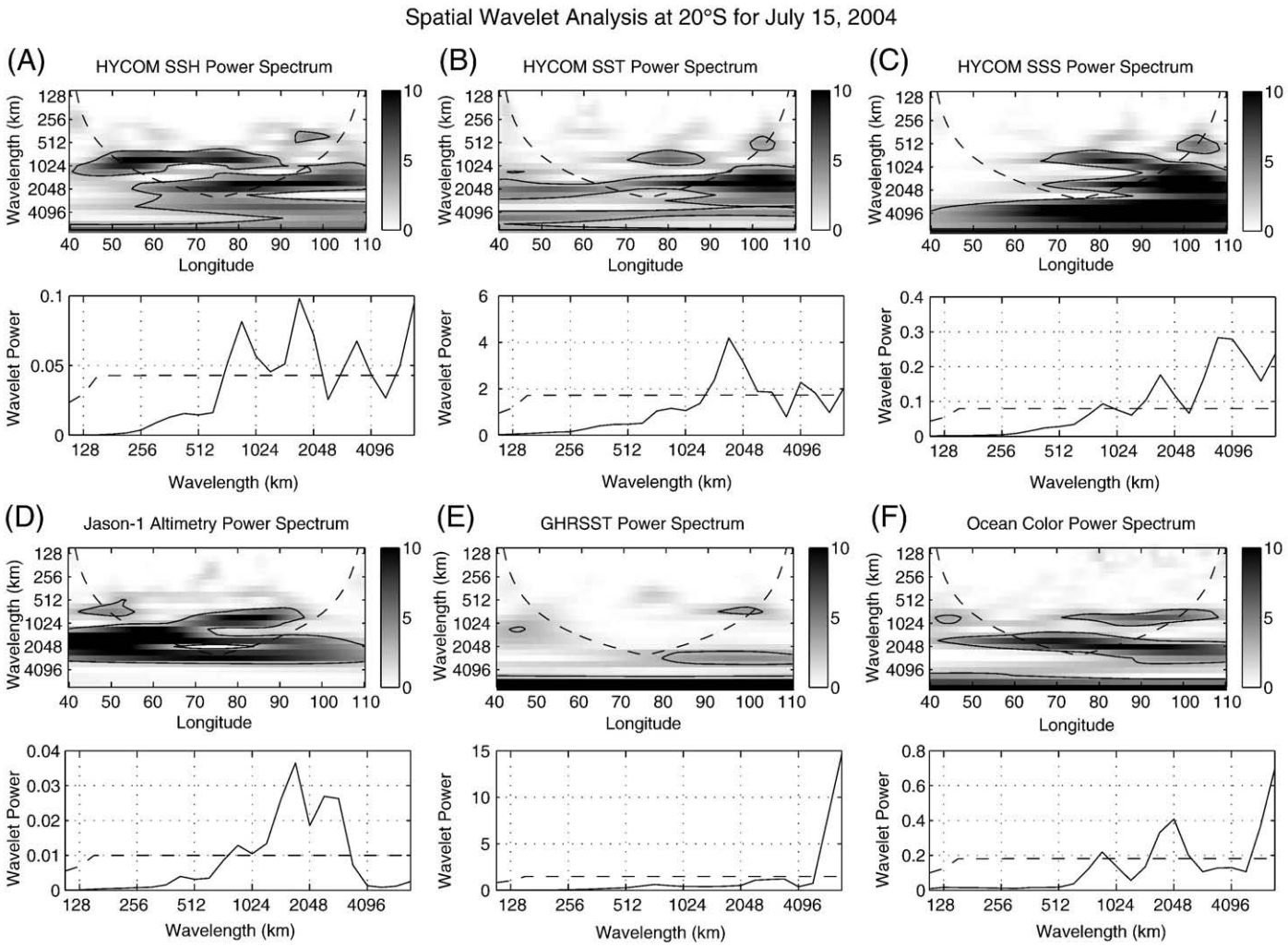

Fig. 8. Wavelet analysis of longitude series extracted from longitude/time plots of parameter anomalies at 20°S for July 15, 2004. The top diagram of each subplot is the wavelet power spectrum (how important a certain wavelength is at a given time). The bottom diagram is of the global wavelet power (how important a particular wavelength is relative to the whole time series). The dashed curve in the power spectrum figures is the cone of influence, below which edge effects become important and results have to be treated with caution. The dashed line in the global power diagrams is the 95% significance level (anything above is considered significant). A) HYCOM SSH, B) HYCOM SST, C) HYCOM SSS, D) Jason-1 altimetry, E) GHRSST, and F) ocean color (log of chl-*a* concentration).

A wavelet analysis was also run in space to get an idea of how the wavelengths of the Rossby waves change while traversing the basin at 20°S. (We also tried a spatial wavelet analysis at 10°S; however, at this latitude the wavelengths of Rossby waves are too long to be resolved, and so fall under the cone of influence below which edge effects become important. The cone of influence is defined formally as the *e*-folding time for the autocorrelation of wavelet power at each scale (Torrence & Compo, 1998). The spatial analysis was done at several times (January 15, 2004 and 2005, and July 15, 2004 and 2005); however, only the July 2004 results are shown (Fig. 8). These times were chosen because: (1) they span the middle of the study period, and so most of the time series of the previous analyses at those times fall above the cone of influence; and (2) the analyses presented in Figs. 6 and 7 (as well as other plots not shown) have strong peaks in the energy plot at those times (not all parameters, however, had strong peaks at the same time).

It is important to note that there is a bathymetric feature called the 90 East ridge in the Eastern Indian Ocean that spans about 50°S to 15°N, running almost directly North–South, with a very slight Eastward component. As the name implies, at its northern end it is near the 90°E meridian (although at 20°S it runs almost parallel to the 88°E meridian).

In July 2004 (Fig. 8), the HYCOM parameters all show a feature with a wavelength of about 2000 km to the east of the ridge that shifts some energy into a shorter wavelength feature of about 800 km upon hitting the ridge and passing over it to the west. In ocean color chl-*a* and GHRSST, the 800 km feature appears on the east of the ridge and dissipates upon hitting it (this feature is barely visible in ocean color chl-*a* largely due to an increasing trend to the east, which appears as the massive >4100 km wavelength signal in the wavelet analysis). This 800 km feature also appears in Jason-1 altimetry and, like the HYCOM parameters (Fig. 9), it strengthens to the west of the ridge. However, instead of it "getting energy" from the 2000 km feature as it crosses the ridge, it appears to provide energy to the longer wavelength feature at about 70°E, well to the west of the ridge.

5. Summary

Rossby waves are difficult to detect with *in situ* methods due to insufficient space-time coverage. However, Rossby waves have thus far been seen in several parameters derived from satellites such as sea surface height (SSH), sea surface temperature (SST) and ocean color observations of chlorophyll-*a* (chl-*a*). Up until this point, nobody has shown that Rossby waves can be seen in global salinity field, largely

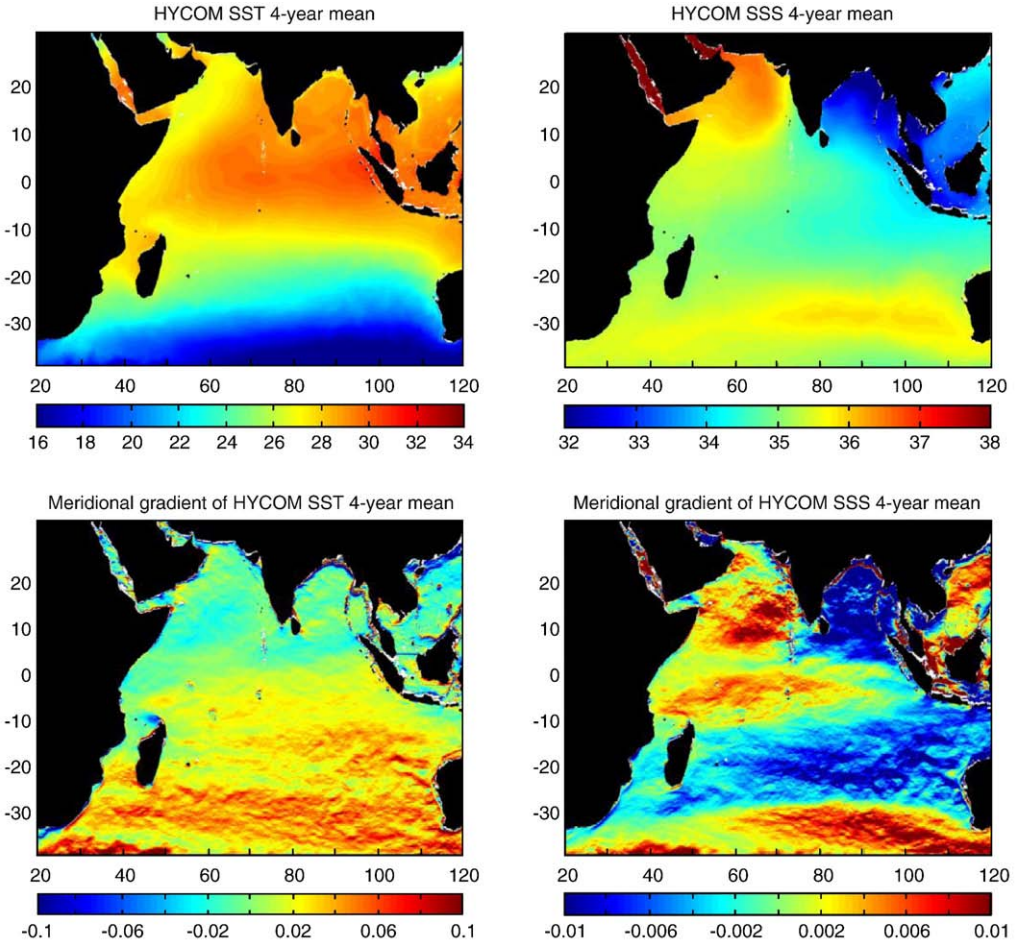

Fig. 9. (Top panel) HYCOM simulations of SST and SSS 4-year mean, and (bottom panel) meridional gradient of HYCOM SST and SSS 4-year mean.

because there is currently no easy way to acquire basin wide salinity data. We did a preliminary study (Heffner et al., 2008) and demonstrated that Rossby waves can be identified in the sea surface salinity (SSS) signal, using HYbrid Coordinate Ocean Model (HYCOM) simulations as a proxy for the awaited satellite-derived salinity data.

Observing Rossby wave signals in salinity will be helpful to better understand these waves. While SST has a strong seasonal signal, salinity is only weakly affected by the changing seasons. It is also problematic observing Rossby waves in ocean color because chlorophyll-*a* depends on various nutrient fields, which are not well known compared with standard physical oceanography fields such as (Evaporation–Precipitation) at the surface. A physical variable with better defined forcings, the variation of salinity should be much easier to understand than for a biological field.

While the structure of Rossby waves can be elucidated from comparisons of the signal in different sea surface parameters, models are needed to gain direct information about how these waves affect the ocean at depth. The first three baroclinic modes of the Rossby waves are inferred from the Fast Fourier Transform (FFT), and two-dimensional Radon Transform (2D RT). At many latitudes the first, second and third baroclinic mode Rossby wave phase speeds from satellite observations and model parameters are identified. Wavelet transforms of these multi-parameters from satellite observations and model simulations help to discriminate between the annual and semi-annual signal of these Rossby waves.

Future salinity missions, notably ESA's Soil Moisture and Ocean Salinity (SMOS) and joint U.S. and Argentina Aquarius missions, will open a new era in Rossby wave studies using high spatial and temporal coverage of satellite-derived salinity. HYCOM SSS range of 0.03–0.3 psu demonstrates that these satellite missions should be able to resolve Rossby waves in SSS at some latitudes.

Acknowledgements

This work was supported in part by the NASA Physical Oceanography Program under Grant NNG06GJ22G awarded to B.S. JS was supported by the 6.1 project "Global and Remote Littoral Forcing in Global Ocean Models" sponsored by the Office of Naval Research (ONR) under program element 601153N. The HYCOM model results were obtained under grants of challenge and non-challenge computer time from the Department of Defense High Performance Computing Program at the Naval Oceanographic Office, Stennis Space Center, MS. We wish to give special thanks to Mr. Jeff R. Blundell for providing helpful comments and discussion that greatly enhanced this paper. We would also like to thank late Prof. Peter Killworth for making the theoretical Rossby wave speed data available. The authors would like to thank two anonymous reviewers for their valuable comments and thorough review.

References

Challenor, P. G., Cipollini, P., & Cromwell, D. (2001). User of the 3D Radon Transform to examine the properties of oceanic Rossby waves. *Journal of Atmospheric and Oceanic Technology*, *18*, 1558—1566.

Charria, G., Dadou, I., Cipollini, P., Drévillon, M., De Mey, P., & Garçon, V. (2006). Understanding the influence of Rossby waves on surface chlorophyll concentrations in the North Atlantic Ocean. *Journal of Marine Research*, *64*, 43—71.

Charria, G., Mélin, F., Dadou, I., Radenac, M. -H., & Garçon, V. (2003). Rossby wave and ocean colour: The cells uplifting hypothesis in the South Atlantic Subtropical Convergence Zone. *Geophysical Research Letters*, *30*, 1125. doi:10.1029/2002/GL016390.

Chelton, D. B., & Schlax, M. G. (1996). Global observations of oceanic Rossby waves. *Science*, *272*, 234—238.
Cipollini, P., Cromwell, D., Challenor, P. G., & Raffaglio, S. (2001). Rossby waves detected in global ocean colour data. *Geophysical Research Letters*, *28*, 323—326.
Cipollini, P., Cromwell, D., Jones, M. S., Quartly, G. D., & Challenor, P. G. (1997). Concurrent altimeter and infrared observations of Rossby wave propagation near 34°N in the Northeast Atlantic. *Geophysical Research Letters*, *24*, 889—892.
Cipollini, P., Cromwell, D., Quartly, G. D., & Challenor, P. G. (2000). Remote sensing of oceanic extra-tropical Rossby waves. In David Halpern (Ed.), *Satellites, oceanography, and society* (pp. 99—123). New York: Elsevier.
Cromwell, D. (2001). Sea surface height observations of the 34°N 'waveguide' in the North Atlantic. *Geophysical Research Letters*, *19*, 3705—3708.
Dandonneau, Y., Vega, A., Loisel, H., du Penhoat, Y., & Menkes, C. (2003). Oceanic Rossby waves acting as a "hay rake" for ecosystem floating by-products. *Science*, *302*, 1548—1551.
Deans, S. R. (1983). *The Radon Transform and some of its applications.* New York: John Wiley.
Foufoula-Georgiou, E., & Kumar, P. (1994). *Wavelets in Geophysics.* San Diego: Academic Press.
Fu, L. L. (2004). Latitudinal and frequency characteristics of the westward propagation of large-scale oceanic variability. *Journal of Physical Oceanography*, *34*, 1907—1921.
Graps, A. (1995). An introduction to wavelets. *IEEE Computational Science & Engineering*, *2*, 50—61.
Heffner, D. M., Subrahmanyam, B., & Shriver, J. F. (2008). Indian Ocean Rossby waves detected in HYCOM sea surface salinity. *Geophysical Research Letters*, *35*, L03605. doi:10.1029/2007GL032760.
Hill, K. L., Robinson, I. S., & Cipollini, P. (2000). Propagation characteristics of extra-tropical planetary waves observed in the ASTR global sea surface temperature record. *Journal of Geophysics Research*, *105*, 21927—21945.
Kawamiya, M., & Oschlies, A. (2001). Formation of a basin-scale surface chlorophyll pattern of Rossby waves. *Geophysical Research Letters*, *28*, 4139—4142.
Kerr, Y., Font, J., Waldteufel, P., & Berger, M. (2000). The second of ESA's opportunity missions: The Soil Moisture and Ocean Salinity Mission — SMOS. *ESA Earth Observation Quarterly*, *66*, 18f.
Killworth, P. D., & Blundell, J. R. (2003). Long extratropical planetary wave propagation in the presence of slowly varying mean flow and bottom topography. Part I: The local problem. *Journal of Physical Oceanography*, *33*, 784—801.
Killworth, P. D., & Blundell, J. R. (2003). Long extratropical planetary wave propagation in the presence of slowly varying mean flow and bottom topography. Part II: Ray propagation and comparison with observations. *Journal of Physical Oceanography*, *33*, 802—821.
Killworth, P. D., Chelton, D. B., & de Szoeke, R. (1997). The speed of observed and theoretical long extratropical planetary waves. *Journal of Physical Oceanography*, *27*, 1946—1966.
Killworth, P. D., Cipollini, P., Uz, B. M., & Blundell, J. R. (2004). Physical and biological mechanisms for planetary waves observed in satellite-derived chlorophyll. *Journal of Geophysics Research*, *109*, C07002. doi:10.1029/2003JC001768.
Lagerloef, G. S. E. (2001). Satellite measurements of salinity. In J. Steele, S. Thorpe, & K. Turekian (Eds.), *Encyclopedia of Ocean Sciences* (pp. 2511—2516). London: Academic Press.
Machu, E., Ferret, B., & Garçon, V. (1999). Phytoplankton pigment distribution from SeaWiFS data in the subtropical convergence zone south of Africa: A wavelet analysis. *Geophysical Research Letters*, *26*, 1469—1472.
Maritorena, S., Siegel, D.A., Hembise Fanton d'Andon, O., Mangin, A. (submitted for publication). Ocean Color Merged Data Sets: Benefits and Challenges. Remote Sens. of Envi.
Meyers, S. D., Kelly, B. G., & O'Brien, J. J. (1993). An introduction to wavelet analysis in oceanography and meteorology: With application to the dispersion of Yanai waves. *Monthly Weather Review*, *121*, 2858—2866.
Perigaud, C., & Delecluse, P. (1992). Annual sea level variations in the southern tropical Indian Ocean from Geosat and shallow-water simulations. *Journal of Geophysics Research*, *97*, 20169—20178.
Polito, P. S., & Liu, W. T. (2003). Global characterization of Rossby waves at several spectral bands. *Journal of Geophysics Research*, *108*, C13018. doi:10.1029/2000JC0000607.
Quartly, G. D., Cipollini, P., Cromwell, D., & Challenor, P. G. (2003). Rossby waves: Synergy in action. *Philosophical Transactions of the Royal Society of London. A*, *361*, 57—63.
Siegel, D. A. (2001). The Rossby rototiller. *Nature*, *409*, 576—577.
Subrahmanyam, B., Robinson, I. S., Blundell, J. R., & Challenor, P. G. (2001). Indian Ocean Rossby waves observed in TOPEX/POSEIDON altimeter data and in model simulations. *International Journal of Remote Sensing*, *22*, 141—167.
Tokmakian, R. T., & Challenor, P. G. (1993). Observations in the Canary Basin and the Azores Frontal region using Geosat data. *Journal of Geophysics Research*, *98*, 4761—4773.
Torrence, C., & Compo, G. P. (1998). A practical guide to wavelet analysis. *Bulletin of the American Meteorological Society*, *79*, 61—78.
Uz, B. M., Yoder, J. A., & Osychny, V. (2001). Pumping of nutrients to ocean surface waters by the action of propagating planetary waves. *Nature*, *409*, 597—600.